Collision-Partner Dependence of Energy Transfer between the CH $A^2\Delta$ and $B^2\Sigma^-$ States

Graham Richmond, Matthew L. Costen, and Kenneth G. McKendrick*

School of Engineering and Physical Sciences, Heriot-Watt University, Edinburgh, EH14 4AS, U.K.

Received: October 6, 2004; In Final Form: November 12, 2004

We have investigated experimentally the collision-induced electronic energy transfer between the CH $A^2\Delta$ and $B^2\Sigma^-$ states with the series of partners He, Ar, H_2, N_2, CO, and CO_2. Single rovibronic states of either of the near-degenerate levels $A^2\Delta$, $v = 1$, or $B^2\Sigma^-$, $v = 0$, were prepared by laser excitation. Collisional transfer processes were monitored by detecting dispersed, time-resolved fluorescence from the initial and product states. The microscopic rate constants for vibronically resolved transfer between the $A^2\Delta$ and $B^2\Sigma^-$ states, vibrational relaxation within the A state, and total removal to unobserved final products were determined for each partner. In line with previous work, we find that only CO and H_2 are efficient at total removal of CH $A^2\Delta$ and $B^2\Sigma^-$, most probably through chemical reaction. CO_2 is notably effective at $A^2\Delta$ state vibrational relaxation, possibly through resonant vibrational energy transfer. All the partners cause transfer between CH $A^2\Delta$ and $B^2\Sigma^-$. An important new observation is that their efficiencies are well correlated with the strength of long-range attractive forces, as revealed through a positive correlation of the Parmenter−Seaver type. The vibronic branching to $A^2\Delta$, $v = 0$ and 1 from $B^2\Sigma^-$, $v = 0$ is found to be significantly collision-partner-dependent and not well predicted by energy gap scaling laws. We do not find any enhanced effectiveness in $B^2\Sigma^-$ to $A^2\Delta$ coupling for those partners which form strongly bound intermediates, suggesting that this specific electronic channel is controlled by different regions of the potential energy surfaces.

Introduction

The CH radical is an important species in many processes in nature. CH is a key intermediate in technological plasmas, such as in the chemical vapor deposition of thin layer synthetic diamond films. It occurs in interstellar space, as well as in the atmosphere of the sun and other stars. Perhaps the most practically significant environment where CH radicals are found, though, is in hydrocarbon combustion. CH plays a key role in this chemistry, including the mechanism of prompt NO formation, and is the source of the bright blue color seen in hydrocarbon flames.

The CH radical has been the subject of thorough spectroscopic measurements[1−4] of its band systems and computational work[5,6] on the corresponding states, particularly the $A^2\Delta$ and $B^2\Sigma^-$ states featured in this work. The A and B states are nearly degenerate, with A ($v = 1$) located a few hundred cm^{-1} above B ($v = 0$), as shown in Figure 1. Each state is optically connected to the ground state, and strong diagonal A−X and B−X transitions are readily observable.

It is because of these spectroscopic properties that there has been much interest in the use of CH radicals as a marker for various properties of flames. Laser-induced fluorescence (LIF) based techniques have been used in measurements of flame temperatures[7,8] and reaction zone imaging.[9−11] To better understand the role of CH in combustion chemistry, LIF and cavity ring down spectroscopy (CRDS) techniques have also been used to measure number densities and profiles of CH radicals in flames.[12−15] It is partly because of its high practical importance that CH is the focus of our work.

There has been much interest in quenching of the $A^2\Delta$ ($v = 0$) state of CH both in flames[16,17] and with various individual collision partners.[18−32] Total removal rates for CH (B and C) by a range of colliders have also been measured.[33] It is much less common in quenching studies for the product state of the quenched molecules to be identified. This can, for example, be a different rotational level in the same vibronic state as in rotational energy transfer (RET), a different vibrational level

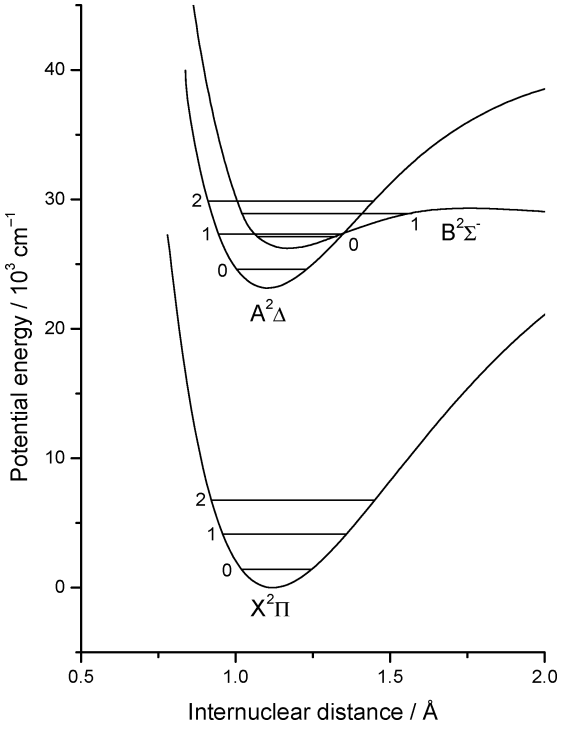

Figure 1. Potential energy curves of the $X^2\Pi$, $A^2\Delta$, and $B^2\Sigma^-$ states of the CH radical, based partly on ab initio calculations.[5]

* Corresponding author. E-mail: K.G.McKendrick@hw.ac.uk. Telephone: +44-131 451 3109. Fax: +44-131 451 3180.

10.1021/jp045444m CCC: $30.25
Published on Web 01/05/2005

in the same electronic state as in vibrational energy transfer (VET), or as in electronic energy transfer (EET), a different electronic state altogether.

RET in A- and B-state CH has been widely studied both in flames[34−38] and in single-collider conditions.[39−48] VET has also been studied in the A and B states of CH.[40,41] The main focus of this work is collision-induced EET, specifically that between the $A^2\Delta$ and $B^2\Sigma^-$ states of CH. This is a known process in the gas phase, and yet, there is no full quantitative understanding of its mechanism. Garland and Crosley first observed collisional coupling between the A and B states of CH in experiments comparing VET, RET, and EET to total removal in atmospheric pressure flames.[34] They found that after initial excitation to B ($v = 0$), emission from A ($v = 1$) with a statistical rotational distribution was detected. The reverse case also occurred; on excitation to A ($v = 0$, 1), emission from B ($v = 0$) was recorded. Rensberger, Dyer, and Copeland later measured time-dependent LIF signals of the CH A and B states in a range of low-pressure flames.[35] After excitation to the B state, directly returning emission was found to have an exponential decay. A-state emission showed an exponential growth due to population by EET from the B state, followed by an exponential decay due to subsequent collisional removal.

Previously, our group has quantitatively studied transfer between the A ($v = 0$, 1) and B ($v = 0$) states of CH, induced by collisions with CO_2. This was the first such study under well-defined temperature and pressure conditions.[49] Prior measurements in flames by their nature were carried out in the presence of a relatively uncharacterized mixture of multiple collision partners and at poorly defined temperatures. We found that transfer occurs between the B ($v = 0$) and A ($v = 0$, 1) levels and in reverse from the A ($v = 1$) to B ($v = 0$) level. A kinetic model was proposed, incorporating transfer between these three vibronic levels, along with total removal processes and radiative transfer to the $X^2\Pi$ ground state. An important finding was that the measured branching ratio for B ($v = 0$) → A ($v = 1$) versus B ($v = 0$) → A ($v = 0$) transfer disagrees strongly with predictions from simple energy gap scaling laws. This work also highlighted potential problems with previous studies where both A- and B-state CH are produced from photolysis and used in kinetics measurements. Collisional B ↔ A mixing will occur between the nascent excited-state populations, leading, for example, to unexpected enhancement of lifetimes for states being populated by EET.

This work was then extended[50] to rotational resolution to determine the correlation between the initial rotational level that was pumped and the product state rotational distribution. It was found that pumping higher rotational levels led to a narrower range of ΔN in the product state than was found when pumping lower rotational levels, but in either case, a broader range of ΔN was seen compared to pure RET measurements. The peak in the product state rotational distributions following EET occurred at the rotational level closest, but lower lying, to that in the initial state. This implies that the collision that causes the electronic state change interacts more strongly with the potential surface than those that bring about rotational energy transfer.

Crosley and co-workers have recently[37] measured B → A transfer between B ($v = 1$) and A ($v = 0$, 1, 2) as part of a wider study of predissociation rates, RET, and VET in CH B ($v = 0$, 1) in atmospheric and low-pressure flames. They measured vibrational branching ratios for transfer into A ($v = 0$, 1, 2) broadly comparable to those measured in our own previous work with CO_2. They found that a more complex exponential gap law, with additional adjustable parameters, was capable of predicting their results.

Subsequently, Kind and Stuhl have observed collisional B → A mixing in a RET investigation of CH B ($v = 0$) with Ar.[43] Collisional mixing between the A and B states was observed at a pressure of ∼40 Torr and deemed to be insignificant at the much lower pressure at which the RET measurements were made. Stuhl and co-workers have also quantitatively measured B → A conversion by collisions with CO,[48] along with rotational relaxation and total removal. B ($v = 0$) → A ($v = 1$) transfer was not resolved from B ($v = 0$) → A ($v = 0$), but a combined rate constant for overall B → A transfer was extracted with a comparatively similar value to our previously measured values for CO_2.

Although these studies have confirmed that B ↔ A coupling is a significant channel for some colliders, there has as yet been no systematic study of the relative efficiencies of other colliders. This provides the motivation for the current work in which we study the effects of He, Ar, H_2, N_2, CO, and CO_2 as collision partners. These include some purely physical colliders, such as Ar and He, and others with potentially reactive channels such as CO and H_2. Our aim is to better understand which regions of the potential energy surface are responsible for controlling the mechanism of electronic energy transfer.

Experimental Section

The experiments were carried out in a stainless steel six-way cross vacuum system, pumped by an Edwards cryotrapped diffusion pump, which was in turn backed by an Edwards E2M18 rotary pump. The collision partners were flowed through an MKS 100 standard cubic centimeters per minute (sccm) mass-flow controller into the chamber via polytetrafluoroethylene (PTFE) gas lines. CH radicals were produced by the UV multiphoton photolysis of bromoform, which was diluted in the collision partner to give a backing pressure of ∼35 Torr, and flowed into the chamber through a needle valve. The diffusion pump was throttled to give a precursor mixture partial pressure of ∼45 mTorr in the chamber, of which approximately 5 mTorr was bromoform. The total pressure was controlled over the range 1−10 Torr by adjusting the flow of the collision partner through the mass-flow controller. Higher-pressure experiments were carried out over the range 15−50 Torr, in a similar way by flowing the collision partner through a needle valve. In this case, the chamber was evacuated only by the E2M18 rotary pump, throttled by an Edwards Speedivalve.

Bromoform was photolyzed using the fourth-harmonic, 266 nm output of a Spectron SL805 Nd:YAG laser. The pulse energy was stable at 65 mJ with a repetition rate of 10 Hz. A delay of 3−5 μs was introduced to allow electronically excited CH radicals produced by the photolysis process to decay to the ground state. The CH radicals were then excited into selected rovibrational levels in either the $A^2\Delta$ or $B^2\Sigma^-$ states using a dye laser system pumped by an Nd:YAG laser (Spectron SL800, SL400G, and SL400EX). The required wavelengths were produced from 532 nm pumping of rhodamine 101 or rhodamine B to give 590−620 nm output. This was then mixed with the residual fundamental output from the Nd:YAG laser in a type II KD*P mixing crystal to give up to 30 mJ in the region of the B−X (0,0) and A−X (1,0) bands from 380 to 390 nm. Both the photolysis and pump beams were mildly focused to diameters of approximately 2.0 and 1.5 mm, respectively, at the detection zone in the chamber.

Fluorescence was passed along a UV liquid light guide (Ultrafine Technology, 8 mm diameter, 500 mm length),

dispersed using a monochromator (Hilger and Watts, Monospek 1000, 1 m), and detected with a photomultiplier tube (PMT) (EMI 9789QB). A second PMT (EMI 9813QB) measured fluorescence through either a 390 or a 430 nm interference filter to isolate directly returning emission following $B^2\Sigma^-$ ($v = 0$) or $A^2\Delta$ ($v = 1$) excitation, respectively. This allowed normalization of the dispersed fluorescence signals to the amount of A- or B-state CH produced by excitation.

Signals were recorded by a computer-controlled CAMAC modular data acquisition system running custom-programmed software. This allowed gate-integrated as well as time-resolved signals to be acquired (100 MHz DSP 2001A transient digitizer, SRS SR250 boxcar integrator, and Hytec 520 A/DC). Laser trigger timings (LeCroy 4222 PDG delay generator) and the scanning of the dye laser and monochromator were also controlled.

The collision partners used were CO_2 (BOC, 99.995%), CO (BOC, 100.000%), N_2 (BOC, 99.995%), Ar (BOC, 99.9995%), He (BOC, 99.9995%), and H_2 (BOC, 99.9995%). The bromoform used was laboratory grade (Fisons), degassed by repeated freeze−pump−thaw cycles.

Results

Selective Excitation to the $A^2\Delta$ and $B^2\Sigma^-$ States. To investigate the coupling of the $A^2\Delta$ and $B^2\Sigma^-$ states, CH radicals were prepared in the nearly degenerate $A^2\Delta$, $v = 1$ and $B^2\Sigma^-$, $v = 0$ levels (labeled hereafter as A1 and B0). In vibronic terms, the A1 level is higher in energy than B0, their lowest rotational levels being separated by 260 cm^{-1}. Transfer to the $A^2\Delta$, $v = 0$ level (similarly, A0) from B0 is significantly exothermic, by 2475 cm^{-1}.

To select suitable transitions for pumping, LIF excitation spectra for the B0 and A1 levels were recorded. The respective total integrated B−X (0,0) or A−X ($\Delta v = 0$) fluorescence intensity was monitored as a function of pump laser wavelength. For excitation to B0, the strong, near-diagonal B−X (0,0) band at 388 nm is the obvious choice. The A−X (1,0) band overlaps with the R branch of B−X (0,0), and although less diagonal, without due care could result in accidental simultaneous population of both the A and B states. Fortunately, the B−X (0,0) $R_1(3)$ line is suitably isolated to allow population of B, $v = 0$, $N = 4$, without any contribution from either A1 or higher rotational levels in B0.

To populate A1, the diagonal A−X (1,1) transition at 430 nm may seem ideal as it has a very high transition probability but, unfortunately, is almost perfectly overlapped with the A−X (0,0) transition. Instead the off-diagonal A−X (1,0) transition can be used, which although less diagonal, still results in a good signal-to-noise ratio as long as relatively high laser pulse energies are used. Selected lines in the R branch are sufficiently isolated from the B−X (0,0) and A−X (2,1) bands to allow clean excitation to A1. The $R_1(1)$ line was therefore used for selective population of A, $v = 1$, $N = 2$. We discuss further below the extent to which rotational relaxation might compete with the other collisional processes.

Dispersed Fluorescence Spectra. *Diagonal Bands.* The dispersed fluorescence spectra were recorded by tuning the pump laser wavelength to either of the two selected rovibronic lines identified above and integrating the total fluorescence signal as a function of emission wavelength transmitted by the monochromator. These measurements were normalized to the undispersed fluorescence signals recorded by the second PMT as described in the Experimental Section.

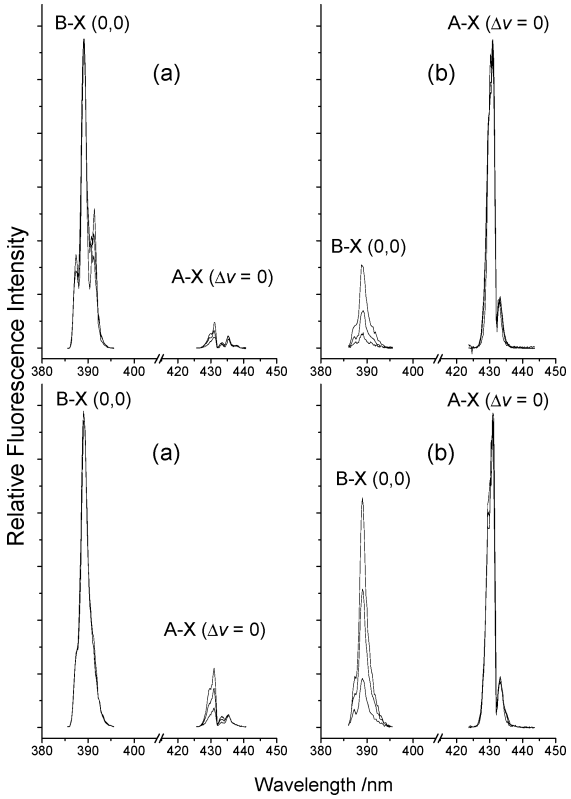

Figure 2. Dispersed fluorescence spectra of the B−X (0,0) and A−X ($\Delta v = 0$) bands in the presence of He (top) and N_2 (bottom): (a) spectra taken following initial excitation to $B^2\Sigma^-$, $v = 0$; (b) spectra recorded following an $A^2\Delta$, $v = 1$ excitation. The spectra shown were taken in the presence of 1, 3, or 6 Torr of collider. In each case, the collisionally populated band grows monotonically with pressure relative to the directly populated band to which they are normalized in each case. Experimental band width is 1.40 nm.

B ↔ A coupling was characterized by a series of measurements where the monochromator was scanned over the diagonal B−X and A−X bands, resulting in emission spectra as shown in Figure 2.

In the case of initial excitation to B0, the collisionally populated A−X ($\Delta v = 0$) band system was integrated over contributing wavelengths and divided by the integral of the directly returning B−X (0,0) band to give the ratio I_A/I_B. The A−X signal was seen to grow with pressure, with varying efficiency depending on the collision partner used. In the case of excitation to A1, the converse occurred. Emission from the B−X (0,0) band grew with pressure of collider and was compared with directly returning emission on the A−X ($\Delta v = 0$) bands to give the ratios I_B/I_A. The experiments were carried out over various pressure ranges depending on the collider used. With colliders such as CO and H_2, experiments could not be carried out at pressures above ~6 Torr as a result of their reactivity toward CH. H_2 is reactive toward the ground state of CH,[33] meaning that in the 3 μs delay between photolysis and pump lasers efficient total removal of the ground-state CH took place, resulting in fewer excited-state CH radicals being created and, therefore, increasingly poor signal-to-noise ratios at higher pressures. CO is less reactive toward ground-state CH[51] but is highly reactive toward A- and B-state CH. This excited state removal competes with the transfer processes and effectively dominates at higher pressures, again resulting in poor signal-to-noise ratios at pressures above around 6 Torr. Experiments with N_2, Ar, and He were carried out over a 1−50 Torr pressure range to show a large variation in the collisionally populated signals with pressure. Experiments with CO_2 showed relatively

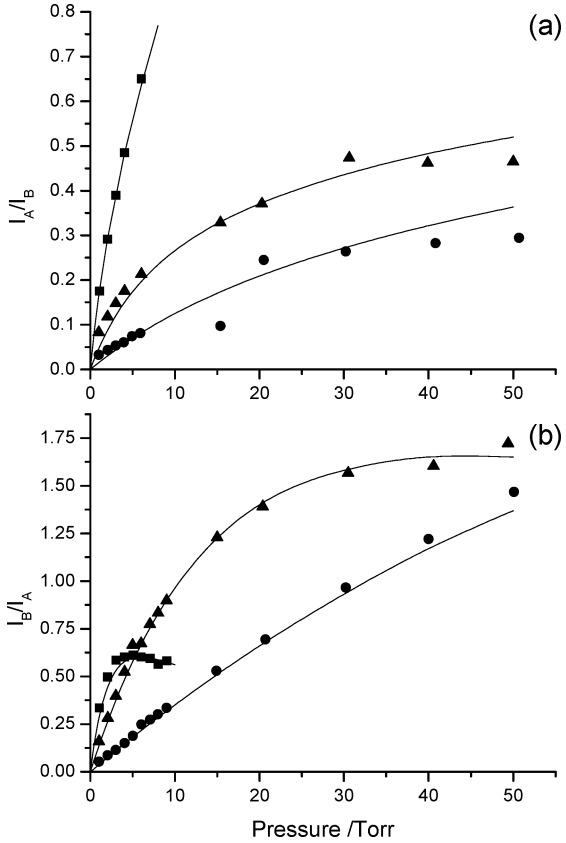

Figure 3. Variation of CH electronic emission intensity ratio with pressure of collider following initial excitation to (a) $B^2\Sigma^-$ ($v = 0$) and (b) $A^2\Delta$ ($v = 1$). In each case squares, triangles, and circles represent experimental results measured for CO_2, N_2, and He, respectively. Ratios are obtained from the integrals of the complete A−X ($\Delta v = 0$) and B−X (0,0) bands, shown, for example, in the spectra in Figure 2. Solid lines represent predictions of the kinetic model described in the text.

large collisionally populated signals even at pressures below 10 Torr; so higher-pressure measurements were deemed unnecessary.

These ratios are plotted in Figure 3 for the representative colliders CO_2, N_2, and He. Similar ratios were also measured with H_2, Ar, and CO but have been omitted from this diagram for clarity. As can be seen from the figure, the ratios measured with N_2 and He show qualitatively similar behavior regardless of which electronic state is initially populated. N_2 has a higher overall efficiency than He. CO_2, in contrast, shows a marked difference between excitation to B0 and A1. In the case of excitation to B0, the I_A/I_B ratio grows approximately linearly with increasing pressure, while on excitation to A1, the I_B/I_A ratio initially rises rapidly but above ~4 Torr flattens out.

These variations in behavior are direct visual evidence of distinct relationships between the underlying microscopic rate constants for different collision partners. We return to their quantitative determination below.

Off-Diagonal Bands. While the diagonal bands described above are ideal for measurement of overall B ↔ A coupling, the A−X ($\Delta v = 0$) system cannot be easily resolved into its (1,1) and (0,0) components. Therefore, no information is obtained on the relative populations of the A1 and A0 levels, necessary to quantify vibrational relaxation from A1 to A0 as well as the B0 → A0/A1 branching ratio. For this purpose the A−X (0,1) and (1,2) bands at ~486 nm were used. Although they have the obvious disadvantage of being approximately 2 orders of magnitude weaker, they can still be detected with an

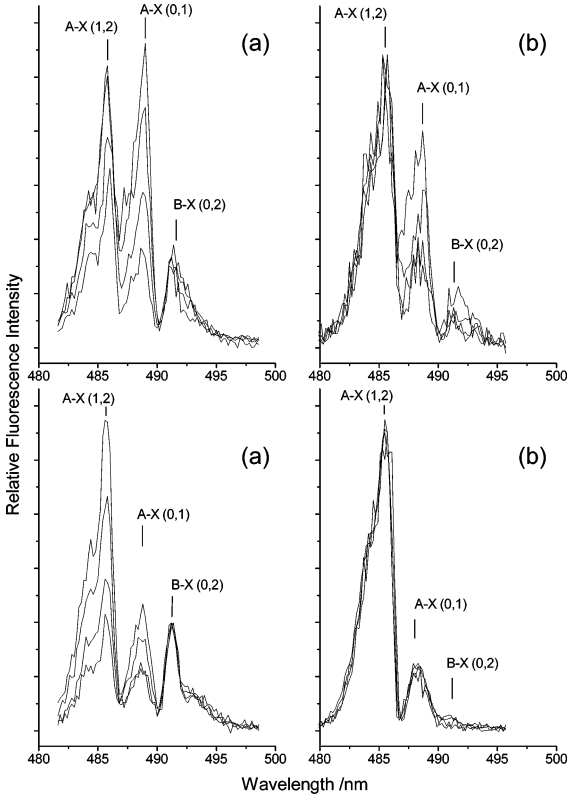

Figure 4. Dispersed fluorescence spectra of the A−X (1,2), A−X (0,1), and B−X (0,2) bands after excitation to (a) $B^2\Sigma^-$ and (b) $A^2\Delta$, in the presence of CO_2 (top) and N_2 (bottom) at pressures between 1 and 6 Torr. Experimental band width is 1.40 nm.

acceptable signal-to-noise ratio. These two bands are separated by 3 nm and also slightly overlapped by the B−X (0,2) band, which is a further order of magnitude weaker.

Figure 4 shows the experimentally measured spectra with varying pressures of CO_2 and N_2. On excitation to B0, emission is seen from both the A−X (1,2) and A−X (0,1) bands with each collider. As expected from the diagonal band measurements, this increases in intensity with pressure. With CO_2, the A−X (0,1) band also increases relative to the A−X (1,2) with pressure, indicating A1 → A0 vibrational relaxation. With N_2 and all of the other colliders used, the A−X (0,1) band does not grow significantly relative to A−X (1,2) with collider pressure. This indicates that for these partners vibrational relaxation within the A state is slow relative to the other competing removal processes.

Although the off-diagonal bands are more isolated from each other than the diagonal bands, they are still not completely separated. To obtain accurate A0/A1 ratios, it is necessary to simulate the A−X (1,2), A−X (0,1), and B−X (0,2) bands with assumed rotational contours.[52] The combined simulation was iteratively compared to the measured spectra to extract vibronic populations. In the case of B0 excitation, the low-pressure limit of these ratios gives the B0 → A1/A0 vibronic branching ratio directly (see Figure 5). The higher-pressure data also contain information on A1 → A0 relaxation. As expected, the ratios obtained from A1 excitation give clearer information on this vibrational relaxation. Because all of the population starts in the A1 level, they contain no A0 contribution at the low-pressure limit. Also, because B0 is only populated through collisions, there is generally a smaller contribution from the B−X (0,2) band in these spectra. They confirm that only CO_2 is effective in causing measurable A1 → A0 relaxation (with the qualification that the resulting A0 signal would be very weak and hard

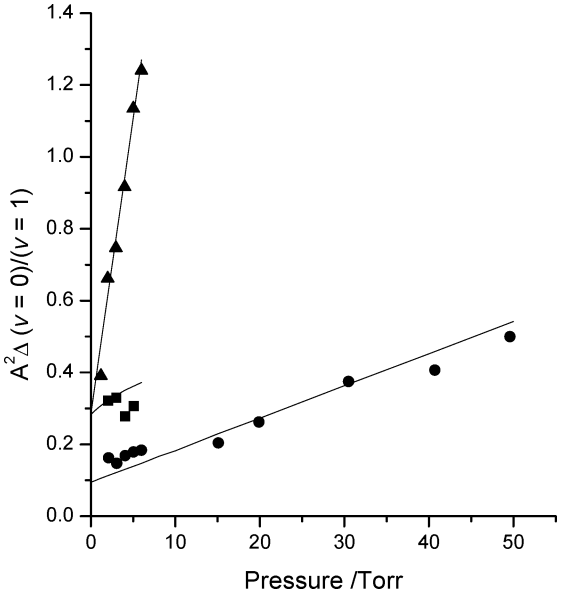

Figure 5. Variation of the $A^2\Delta$ ($v = 0$)/($v = 1$) emission intensity ratio with pressure following initial excitation to $B^2\Sigma^-$ ($v = 0$) in the presence of CO_2 (triangles), H_2 (squares), and N_2 (circles). Solid lines are predictions of the kinetic model using the rate constants in Table 1.

to determine accurately when vibrational relaxation is in competition with very efficient total removal, as is the case for CO and, to a lesser extent, H_2).

Time-Resolved Dispersed Fluorescence. The time dependence of the fluorescence signals was measured by fixing the dye laser and monochromator wavelengths and the relative timing of the lasers. The fluorescence waveform emitted following the dye laser pulse was digitized at 10 ns intervals. Figure 6 shows representative B−X (0,0) and A−X (1,2) waveforms recorded in the presence of 6 Torr N_2 and CO, following excitation to B0 and A1, respectively.

The B−X (0,0) waveforms were recorded by setting the monochromator to transmit the band head at 388 nm and averaging for 1000 shots. The weaker A−X (1,2) waveforms were taken from the R-branch shoulder of the band at 484 nm, to minimize any contribution from underlying A0 emission, and averaged for 10 000 shots. In each case, the directly populated signal (e.g., B−X (0,0) following excitation to B0) shows a very sharp rise following population by the laser followed by decay due to collisional and radiative removal. Conversely, the collisionally populated signals (i.e., A−X (1,2) following excitation to B0) show the expected more gradual rise followed by collisional and radiative decay. The examples in the figure show a marked difference in the overall lifetimes of the signals in the presence of CO and N_2, showing a qualitatively much higher total rate of removal by CO than by N_2. We address the quantitative extraction of all the microscopic rate constants in the next section.

Extraction of Kinetic Parameters. As explained in detail in our previous study with CO_2 as the sole collider,[49] when rotational effects are neglected, these vibronically resolved results can be modeled reasonably satisfactorily on the basis of a four-level kinetic model. This is illustrated in Figure 7.

The individual microscopic bimolecular rate constants for specific collision-induced transitions between vibronic levels are indicated beneath solid arrows. Note that a removal terminating in the final state "X" does not necessarily imply quenching to the electronic ground state. It includes all processes

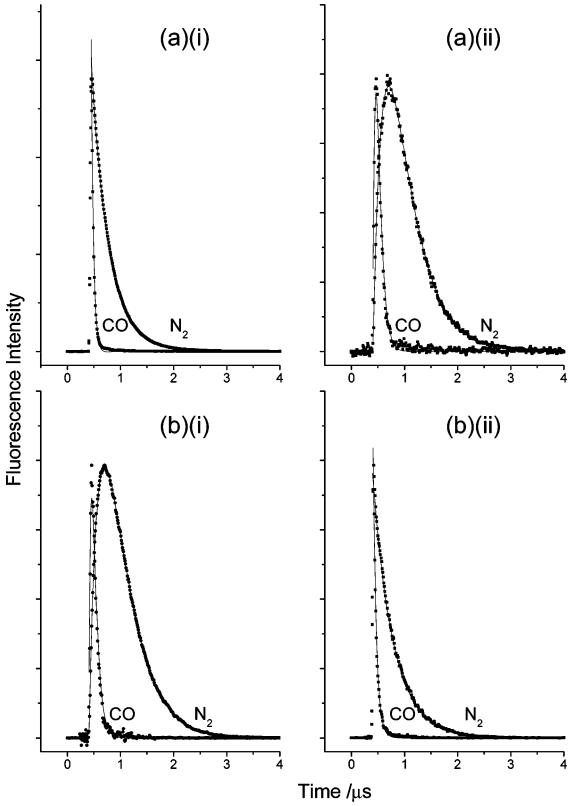

Figure 6. Time dependence of (i) B−X (0,0) and (ii) A−X (1,2) fluorescence, following initial excitation to (a) $B^2\Sigma^-$, $v = 0$ and (b) $A^2\Delta$, $v = 1$. Measurements were taken in the presence of 6 Torr of N_2 and CO, as indicated, and scaled to a common maximum value. Points are experimentally measured data; solid lines are fits to multiexponential functions.

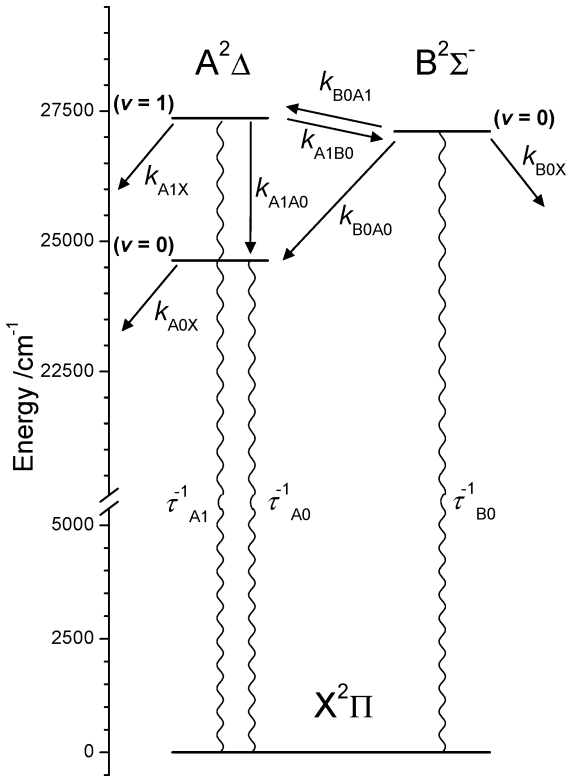

Figure 7. Kinetic scheme showing the collisional and radiative processes involved in the analysis.

for which the final products are in neither the A nor B state and are, therefore, not observed in emission in this study.

Radiative processes are labeled by the corresponding rate (inverse lifetime) and indicated by wavy lines.

We have previously derived[49] the equations governing the time-dependent populations of the pumped level, the near-degenerate reversible collisionally populated level, and the irreversibly populated lower level A0, for each of the cases of initial population of B0 or A1, respectively. For example, in the case of B0 pumping these are

$$N_{B0}(t) = \frac{N_0}{\lambda_1 - \lambda_2}((k_{B0}^T + \lambda_1)\, e^{\lambda_2 t} - (k_{B0}^T + \lambda_2)\, e^{\lambda_1 t}) \quad (1)$$

$$N_{A1}(t) = \frac{N_0 k_{B0\rightarrow A1} P_Q}{\lambda_1 - \lambda_2}(e^{\lambda_1 t} - e^{\lambda_2 t}) \quad (2)$$

and

$$N_{A0}(t) = \frac{N_0}{\lambda_1 - \lambda_2} \times \left\{ \frac{\left(k_{B0\rightarrow A0} P_Q \left(k_{B0}^T + \lambda_1\right) - k_{A1\rightarrow A0} k_{B0\rightarrow A1} P_Q^2\right)}{k_{A0}^T + \lambda_2} \left(e^{\lambda_2 t} - e^{-k_{A0}^T t}\right) - \frac{\left(k_{B0\rightarrow A0} P_Q \left(k_{B0}^T + \lambda_2\right) - k_{A1\rightarrow A0} k_{B0\rightarrow A1} P_Q^2\right)}{k_{A0}^T + \lambda_1} \left(e^{\lambda_1 t} - e^{-k_{A0}^T t}\right) \right\} \quad (3)$$

Those for A1 pumping are related by a simple exchange of the B0 and A1 labels throughout.

In these expressions, N_0 represents the initial number density of either A- or B-state CH radicals created by the pump laser. P_Q is the collision partner number density, and t is the time scale of the experiment.

There are two key sets of kinetics parameters that appear in these expressions. The first is the three pseudo-first-order total removal rate constants for the respective B- and A-state vibronic levels:

$$k_{B0}^T = {\tau_{B0}}^{-1} + (k_{B0\rightarrow A1} + k_{B0\rightarrow A0} + k_{B0\rightarrow X})P_Q \quad (4)$$

$$k_{A1}^T = {\tau_{A1}}^{-1} + (k_{A1\rightarrow B0} + k_{A1\rightarrow A0} + k_{A1\rightarrow X})P_Q \quad (5)$$

$$k_{A0}^T = {\tau_{A0}}^{-1} + k_{A0\rightarrow X} P_Q \quad (6)$$

The second is the pair of exponential parameters, λ_1 and λ_2, which are the two roots of the following equation:

$$\lambda_{1/2} = -\frac{1}{2}[(k_{B0}^T + k_{A1}^T) \pm \sqrt{(k_{B0}^T - k_{A1}^T)^2 + 4k_{A1\rightarrow B0} k_{B0\rightarrow A1} {P_Q}^2}] \quad (7)$$

Both λ_1 and λ_2 are negative, with λ_2 having the larger absolute value. An important and useful constraint is that the sum of λ_1 and λ_2,

$$|\lambda_1 + \lambda_2| = (k_{B0}^T + k_{A1}^T) \quad (8)$$

equals the combined total removal rate from the collisionally coupled B0 and A1 levels.

We have also previously rationalized[49] our preferred logical sequence, out of a number which were attempted, for extracting the kinetic parameters from the combined dispersed fluorescence and time-resolved data. In summary, we find the most robust method to obtain λ_1 and λ_2 is to fit to the collisionally transferred waveforms. Our experimental measure of the time-dependent A1 population is the A−X (1,2) waveform obtained following B0 pumping. At a given pressure, performing a nonlinear least-squares fit[53] of eq 2 to these data will therefore yield values for λ_1 and λ_2 at that pressure, as plotted, for example, in Figure 8 for N_2. This requires no knowledge of relative band strengths and is generally a well-conditioned fit, with error limits on the fitted parameters ranging from 0.5 to 2%.

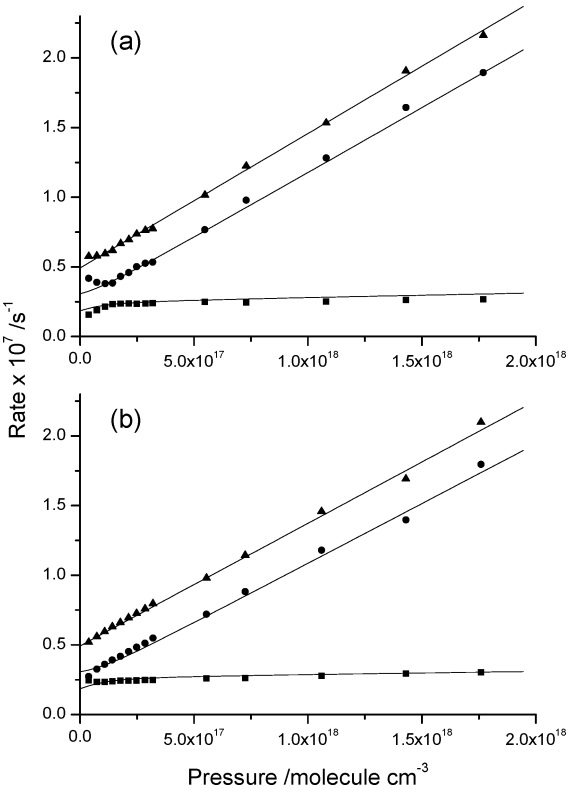

Figure 8. Variation of the kinetic parameters $|\lambda_1|$ (squares), $|\lambda_2|$ (circles), and $|\lambda_1 + \lambda_2|$ (triangles) with pressure of N_2: (a) values obtained from least-squares fits of eq 2 to time-resolved A−X (1,2) emission measurements following excitation to B0, at varying pressures of N_2; (b) values similarly obtained from fits to time-resolved B−X (0,0) emission following A1 pumping. The solid lines in each plot are the predictions of the kinetic model based on the microscopic rate constants shown in Table 1.

The built-in redundancy in having made measurements with both B0 and A1 as initial level provides a useful check on self-consistency. This is illustrated in Figure 9, where the independent pairs of results for $|\lambda_1 + \lambda_2|$ from B0 and A1 pumping for each collider are plotted.

It is then possible to make a fit of eq 1 (or its equivalent) to the waveforms from the initially populated level, of the type shown in Figure 6ai. In this fit, λ_1 and λ_2 are constrained at the individual values obtained at that pressure as shown in Figure 8 for N_2. This process is statistically reliable because random uncertainties in the λ_1 and λ_2 values are generally small, as is obvious from Figure 8, and probably exceeded by any systematic errors. In the fit to eq 1, only the coefficients of the two exponential terms are varied (note that both $(k_{B0}^T + \lambda_1)$ and $-(k_{B0}^T + \lambda_2)$ are positive quantities). Hence, k_{B0}^T and k_{A1}^T are determined from the decays from the initially prepared B0 and A1 levels, respectively. The results are displayed in Figure 10. A typical error in the slope of a straight-line fit through these points is of the order of 5−10%. An indirect value for the other total removal rate constant is then implied in each case by difference from $|\lambda_1 + \lambda_2|$.

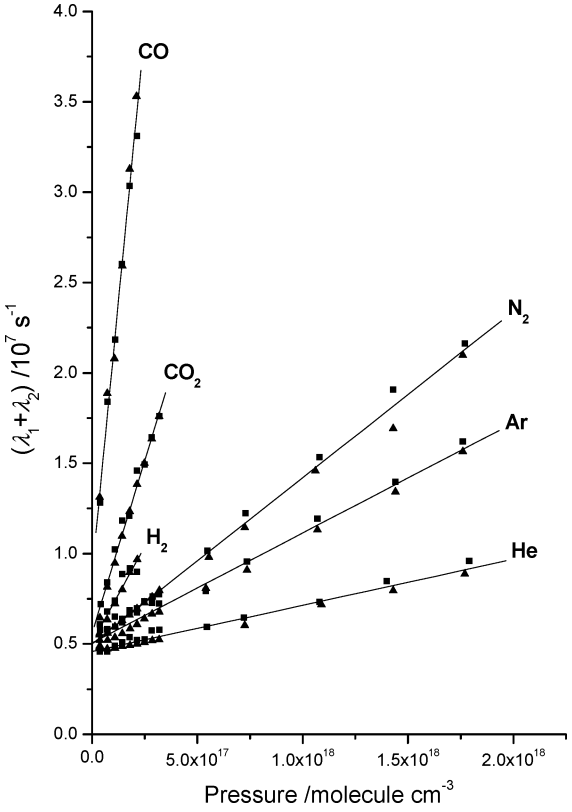

Figure 9. Variation of the kinetic parameter $|\lambda_1 + \lambda_2|$ with pressure of collision partner, obtained from fits to the time dependent fluorescence of the collisionally populated A−X (1,2) band (squares) following excitation to $B^2\Sigma^-$ ($v = 0$) and the B−X (0,0) band (triangles) following initial excitation to $A^2\Delta$ ($v = 1$). Straight lines are simultaneous fits to both sets of data for a given collision partner.

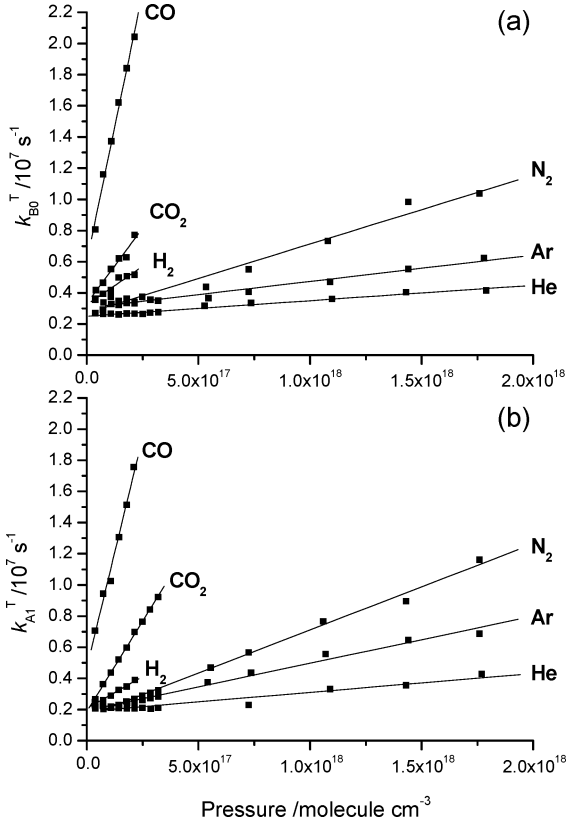

Figure 10. Variation of the kinetic parameters (a) k_{B0}^T and (b) k_{A1}^T with collider pressure, obtained from fits of the directly returning time-resolved fluorescence from the B−X (0,0) and A−X (1,2) bands, respectively. Fits are constrained to the kinetic parameters λ_1 and λ_2.

The slopes, dk_{B0}^T/dP_Q and dk_{A1}^T/dP_Q, of these pseudo-first-order rate constants tabulated in Table 1 define the total bimolecular rate constant for removal from B0 and A1, respectively. Their final subdivision into the respective component bimolecular microscopic rate constants is achieved by iterative comparison of the model predictions with the measured ratios of populations from dispersed fluorescence spectra, such as those in Figures 3 and 5. We have continued to analyze the data sets from B0 and A1 pumping separately, regarding the final level of agreement as a check on the self-consistency of the derived rate constants. We have kept the requirement for the relevant individual rate constants to sum to the respective measured values of $|\lambda_1 + \lambda_2|$ as a firm overall constraint in each case. The summations to the less well-determined individual values of k_{B0}^T and k_{A1}^T were not separately constrained. These, therefore, provide another consistency check.

In fact, some indication of the correct subdivision is contained in the values of λ_1 and λ_2 themselves. For a given sum of the pair, their separate values are sensitive to the makeup of the total removal from either B0 or A1. If this is dominated by reversible B0 ↔ A1 coupling, λ_1 becomes almost independent of pressure and the slope of λ_2 approaches that of $k_{B0}^T + k_{A1}^T$. In the other extreme, loss on unobserved channels dominates. In this case, λ_1 becomes uniquely identified with the smaller of k_{B0}^T and k_{A1}^T, and λ_2 becomes identified with the larger. This would be a good indicator that significant values for the rate constants k_{B0X} and k_{A1X} are required.

Nevertheless, in the majority of real cases, the pressure-dependent ratios of bands in the dispersed fluorescence spectra are a more sensitive measure of the rate constants for B0 ↔ A1 coupling. No prior assumptions were made about the relationship of k_{B0A1} to k_{A1B0}, so this provides an independent check of whether microscopic reversibility is satisfied. In contrast to the purely kinetic data, this analysis does have the potential disadvantage of relying on a prior knowledge of radiative decay rates and relative band strengths. In correcting modeled populations to allow them to be compared directly with measured signals, we have multiplied by the emission coefficients of the various bands involved. This provides a conceivable source of systematic error. The emission coefficients are taken from the literature[54,55] and have values of 2.963×10^6, 1.832×10^6, and 1.676×10^6 s^{-1} for the B−X (0,0), A−X (0,0), and A−X (1,1) bands, respectively. For these stronger diagonal bands, the quoted[54] uncertainties are relatively small, typically of order of 3%. The results would also be affected by any unsuspected strong variation in the detection sensitivity of our apparatus as a function of wavelength over the ∼40 nm between the bands. We have explored the effects of varying this from unity for the B−X (0,0) and A−X ($\Delta v = 0$) emissions. Although it is always possible to improve the fit to either set of data independently this way, we did not find that a bias in either direction produced a significant improvement in the overall fit to the B0 and A1 pumped data taken together.

As noted above, the vibronic branching ratio k_{B0A1}/k_{B0A0} for B0 → A1/A0 transfer is best determined from the low-pressure limiting off-diagonal band (see Figure 5) when B0 is initially prepared. Similarly, the most reliable A1 → A0 vibrational relaxation rate constant will be obtained from the same data when A1 is pumped. In contrast to the diagonal bands, though, the relative band strengths of these much weaker emissions may conceivably be subject to more significant uncertainties, quoted[54] at around 5−10%. Modeled populations were again corrected using the corresponding emission coefficients[54] of 3.546×10^4

TABLE 1: Best-Fit Microscopic Rate Constants/10^{-11} cm^3 molecule^{-1} s^{-1} for All Collision Partners

rate constant	state pumped	value[a]/10^{-11} cm^3 molecule^{-1} s^{-1} He	Ar	H_2	N_2	CO	CO_2
k_{B0A1}	B0	0.10	0.23	0.30	0.35	1.00	1.15
	A1	0.04	0.13	0.30	0.25	1.00	0.85
							1.00[b]
k_{B0A0}	B0	0.02	0.02	0.13	0.05	0.50	0.50
	A1	0.01	0.01	0.13	0.03	0.50	0.37
							0.50[b]
k_{A1B0}	B0	0.15	0.35	0.45	0.52	1.20	1.65
	A1	0.20	0.48	0.55	0.60	1.00	2.00
							1.80[b]
k_{A1A0}	B0	0	0	0[c]	0	0[c]	0.40[d]
	A1	0	0	0[c]	0	0[c]	0.70[d]
							0.70
k_{B0X}	B0	0	0	0.50	0	5.80	0
	A1	0	0	0.80	0	6.50	0
k_{A1X}	B0	0	0	0.50	0	3.00	0
	A1	0	0	0.60	0	3.50	0
k_{A0X}	B0	0	0	0.50	0	3.00	0
	A1	0	0	0.60	0	3.00	0
Pressure Dependence[e]							
$d\|\lambda_1+\lambda_2\|/dP_Q$ [f]	B0	0.27	0.61	1.87	0.96	11.52	3.70
	A1	0.24	0.61	2.37	0.88	12.48	3.93
dk^T_{B0}/dP_Q, [g] measured[h]	B0	0.10	0.21	0.98	0.44	6.90	1.93
dk^T_{B0}/dP_Q, [g] predicted[i]	B0	0.12	0.25	0.93	0.40	7.30	1.65
dk^T_{A1}/dP_Q, [j] measured[h]	A1	0.12	0.30	0.82	0.55	5.90	2.30
dk^T_{A1}/dP_Q, [j] predicted[i]	A1	0.20	0.48	1.15	0.48	4.50	2.70

[a] Systematic and statistical uncertainties can be inferred from the variation in independently measured pairs of values obtained from pumping either the A1 or B0 levels. [b] Taken from ref 49. [c] Values are uncertain within our detection sensitivity due to rapid total removal from the A1 and A0 levels. [d] Pumping A1 provides the most reliable value for k_{A1A0} as the A1 population is created directly rather than by collisional transfer via k_{B0A1}. [e] Slopes of linear fits to the pressure dependence of these kinetic parameters, corresponding to bimolecular rate constants. [f] Values obtained from fits of eq 2 to time-resolved data for the collisionally populated A−X (1,2) in the case of B0 pumping. Similarly, for A1 pumping, an equivalent version of eq 2 is fit to time-resolved B−X (0,0) waveforms. Values are equivalent to the sum of rate constants ($k_{B0A1} + k_{B0A0} + k_{A1B0} + k_{A1A0} + k_{B0X} + k_{A1X}$). [g] Values are equivalent to the sum of rate constants ($k_{B0A1} + k_{B0A0} + k_{B0X}$). [h] Measured k^T_{B0} values obtained from fits of eq 1 to time-resolved B−X (0,0) data following B0 pumping, constrained by relevant λ_1 and λ_2 values. Measured k^T_{A1} values obtained from fits of an equivalent version of eq 1 to time-resolved A−X (1,2) data following A1 pumping. [i] Predicted k^T_{B0} values obtained from the sum of the microscopic rate constants k_{B0X}, k_{B0A1}, and k_{B0A0} shown in the table for B0 pumping. Predicted k^T_{A1} values are similarly calculated from the sum of k_{A1X}, k_{A1B0}, and k_{A1A0} from A1 pumping. [j] Values are equivalent to the sum of rate constants ($k_{A1B0} + k_{A1A0} + k_{A1X}$).

and 5.381×10^4 s^{-1}, for the A−X (0,1) and (1,2) bands, respectively. There is also a particular problem, noted above, in detecting A1 → A0 relaxation reliably when total removal of the A state is especially rapid. For those partners (H_2 and CO) that do cause significant total removal from the A state, we only rather indirectly measure the total removal rate constant from the A0 level, k_{A0X}. It has only a modest influence on the observed ratios of diagonal band emission in Figures 2 and 3. Within these data, the sensitivity following B0 pumping is higher than that for A1 where, in the absence of any perceptible A1 → A0 relaxation, sequential A1 → B0 → A0 transfer is needed to populate A0. We would not, therefore, necessarily expect our k_{A0X} values to be particularly accurate.

The final best-fit values of the rate constants we have derived are collected in Table 1, along with selected cumulative sums for comparison. As noted above, the data derived from B0 and A1 pumping are listed separately throughout. The general overall level of consistency between them is quite satisfactory. The ranges spanned by the independent data provide a good indication of the overall systematic and statistical uncertainties in the individual parameters. The largest relative discrepancies tend to be for the less efficient colliders, particularly He and Ar, for which the transferred signals are correspondingly weaker.

The independent sums $|\lambda_1 + \lambda_2|$ from the B0 and A1 data are in generally excellent agreement, as already indicated by the data in Figure 8. The largest deviation is for H_2, which was restricted to a limited pressure range for the reasons already described. There is naturally little difference, beyond rounding error, between each of the experimental values (fits to the transferred waveforms) of $|\lambda_1 + \lambda_2|$ and the sum over the final derived individual rate constants, because we have imposed this as a constraint.

There is, as expected, somewhat greater variation between the independent experimental values of k^T_{B0} and k^T_{A1} (derived from the fits to respective directly returning waveforms). There is also some scatter of the sums over the final component individual rate constant around these values. As noted above, reproduction of these parameters was not imposed as a separate constraint.

In fact, we believe it is quite likely that the remaining discrepancies between B0 and A1 data sets are the result of systematic effects rather simply of statistical fluctuations in the data. A prime source lies in the neglect of the distribution over rotational levels in the analysis, as we have noted in our original measurements with CO_2.[49] We prepare a single initial rotational level in each of the B0 and A1 levels. Subsequently, collisional vibronic transfer (and total removal) will be in competition with rotational equilibration within the initial vibronic level and radiative loss. The extent to which equilibration is achieved in practice will therefore be a function of pressure in a way that is dependent on the collision partner. Our previous results[50] suggest that this process will not be complete, especially at lower pressures and for the collision partners with more efficient removal channels. Examined in detail, the two rovibronic levels we have prepared initially, $N = 2$ in A1 and $N = 4$ in B0, are very nearly degenerate, consistent with the zero point of the B0 level lying below the A1 level. Rotational equilibration within the A1 state will therefore tend to spread population to higher energy levels than in the B0 state. Consequently, the net transfer rate from A1 to B0 will *increase* as rotational equilibration proceeds, whereas that of the reverse B0 to A1 process will correspondingly *decrease*. It is therefore not surprising that there is some difficulty in finding single values of the parameters k_{B0A1} and k_{A1B0} that satisfactorily reproduce both the A1 and B0 pumped data simultaneously over the full range of pressures. As noted before,[49] this also causes difficulties with testing for microscopic reversibility. Consistent with this, there is considerable scatter in the k_{B0A1}/k_{A1B0} ratio, although for B0 pumping they are somewhat more constant at a value of ~0.7. This does not, however, reproduce particularly well the calculated value[49] of 0.38 for a room-temperature rotational distribution.

Finally, there is an additional potential oversimplification in the analysis in the neglect of return transfer on the channel A0 → B0. Although in vibronic terms this is highly endothermic, our rotationally resolved data[50] for CO_2, at least, suggest that high-lying, nearly degenerate rotational levels in A0 are the initial products. It is therefore possible in principle that some of this population may be collisionally returned to B0 before being rotationally relaxed to lower levels in the A0 state.

Despite these qualifications of finer details of the analysis, which we state for completeness, we nevertheless believe that the values of the microscopic rate constants in Table 1 are sufficiently consistent to reveal quite clearly the general trends among the collision partners. This was the main purpose of this work, the implications of which we discuss further below.

Discussion

There are only two relatively complete previous sets of microscopic rate constants with which we can compare our current results in Table 1: our own previous work on CO_2 [49] and the measurements of Stuhl and co-workers[47,48] on CH (A) and CH (B) quenching by CO.

Not surprisingly, since the methods are essentially identical other than minor refinements in the technique and analysis, our current results for CO_2 differ only modestly from those published previously.[49]

Some slight care is needed to ensure that equivalent quantities are being compared when relating our data to the entirely independent results of Stuhl and co-workers for CO. They have made rotational level-selective measurements of both pure rotational energy transfer within the initial vibronic level and electronic quenching out of this level for both CH (B, $v = 0$)[48] and CH (A, $v = 0$).[47] For CH (B, $v = 0$) they have also observed specific transfer into CH (A), although they were not able to resolve fully the branching between product vibrational levels. Conveniently, they have also reported weighted averages of the rate constants corresponding to thermalized rotational distributions. However, as noted above, the very rapid total removal rates for CO make it the most likely case where full rotational equilibration will not be achieved in our measurements.

The most direct comparisons with Stuhl's data are possible for the B0 level. Our combined total rate constant for removal by CO is the sum of the measured quantities $k_{B0X} + k_{B0A0} + k_{B0A1}$. From Table 1, this spans the range $(7.3-8.0) \times 10^{-11}$ $cm^3\ s^{-1}$ for B0 and A1 pumped data. This is nominally for initial population of $N = 4$ for B0 pumping, although at least some partial rotational relaxation may compete, as discussed above. In comparison, the equivalent quantity is Stuhl's sum of rate constants $k_{q,B} + k_{q,B\rightarrow A}$. This has a value of $(8.9 \pm 0.4) \times 10^{-11}$ $cm^3\ s^{-1}$ for $N = 4$, which differs little from that of 9.6×10^{-11} $cm^3\ s^{-1}$ for a thermally averaged rotational distribution.[48] There is therefore apparently quite reasonable agreement, within ~20%, between our independent results for total removal of the B0 level. In addition, Stuhl's state-specific quantity $k_{q,B\rightarrow A} = (1.42-1.44) \times 10^{-11}$ $cm^3\ s^{-1}$ can be compared directly with our sum over the vibrational channels contributing to B0 to A-state conversion, $k_{B0A0} + k_{B0A1} = 1.5 \times 10^{-11}$ $cm^3\ s^{-1}$ (in both cases of B0 and A1 pumping) again in quite satisfactory agreement.

For CH (A) + CO, Stuhl's group have measured[47] total removal of the A0 level. They find, averaged over a thermal rotational distribution, $k_{q,A} = 5.6 \times 10^{-11}$ $cm^3\ s^{-1}$. As noted above, our data are not especially sensitive to this quantity. Our estimate from Table 1 is 3.0×10^{-11} $cm^3\ s^{-1}$, apparently somewhat lower than found by Stuhl. However, as we have also noted, it is quite likely that the A0 population initially produced from transfer from the B0 level lies in higher rotational levels. Stuhl's data show a rapid decline in total removal, $k_{q,A}$, with increasing N. It is therefore at least qualitatively consistent that we should measure a lower value for k_{A0X}, reflecting only partial rotational equilibration within the collisionally populated A0 state. For the A1 level, for which we have more direct measurements that refer to the lower-lying rotational levels, we find a combined total removal rate constant $k_{A1X} + k_{A1B0}$ $(+k_{A1A0}) = (4.2-4.5) \times 10^{-11}$ $cm^3\ s^{-1}$. This does approach somewhat more closely the value of $k_{q,A}$ measured by Stuhl for A0. There is, of course, no fundamental reason these A1 and A0 rate constants should be equal, and it would be a matter of debate (see below) whether the two significantly contributing channels for A1 should be considered as additive or competitive.

More generally, our results confirm the conclusions reached in a number of previous studies[16,23,28,33,47,48] that only the collision partners CO and H_2 cause relatively rapid total removal of CH (B) and CH (A). It is conceivable that the respective k_{B0X}, k_{A1X}, and k_{A0X} and rate constants contain contributions from quenching to the electronic ground state, $X^2\Pi$, or even, in principle, the lower-lying $a^4\Sigma^-$ state. We reiterate that we have no direct evidence for the end products of any of these removal processes. It is very likely, though, that a significant fraction of the removal in each of these cases is through chemical reaction. For both quenchers there are exothermic channels that are spin-allowed and do not involve chemically unreasonable reorganizations. For CO these include

$$CH\ (B^2\Sigma^-, v = 0) + CO \rightarrow C_2H\ (X^2\Sigma^+) + O(^3P) \qquad \Delta H^\circ_{298K} = -67\ kJ\ mol^{-1} \quad (Ia)$$

$$\rightarrow HCO\ (X^2A') + C(^3P) \qquad \Delta H^\circ_{298K} = -33\ kJ\ mol^{-1} \quad (Ib)$$

with the deeply bound HCCO intermediate lying some 617 kJ mol^{-1} below the reactants. For H_2 there is the exothermic H-atom exchange reaction

$$CH\ (B^2\Sigma^-, v = 0) + H_2 \rightarrow CH_2\ (^3\Sigma_g^-) + H(^2S) \qquad \Delta H^\circ_{298K} = -299\ kJ\ mol^{-1} \quad (II)$$

with the ground state of CH_3 bound by 758 kJ mol^{-1} relative to the reactants. The channel producing singlet CH_2 ($^1A_1$) is only slightly less exothermic by around 37 kJ mol^{-1}.

There are previous reports[23,24,33] of modest, but nonnegligible, total quenching for the other molecular quenchers N_2 and CO_2. We are not necessarily disputing this, but our own measurements are simply not sufficiently sensitive to these minor channels in the presence of relatively more efficient B0 ↔ A1 coupling. We have therefore reported zero values for k_{B0X}, k_{A1X}, and k_{A0X} in Table 1. The previous nonzero values are most likely to be reliable for the lower-lying A0 level, which, as much discussed above, has no energetically accessible channel to the B state. For both these quenchers there are reactive channels that are feasible on energetic grounds. However, we do not discuss further here the possible dynamical reasons for the relatively low rate constants.

When we turn to the rate constants k_{A1A0}, a notable feature of the data in Table 1 is that CO_2 is the only partner for which significant pure vibrational relaxation within the A state is measurable. This was indeed obvious by inspection of the raw off-diagonal dispersed fluorescence spectra, as illustrated in Figure 4. As we have admitted, though, our measurements are not so sensitive to pure vibrational relaxation when it is in competition with rapid total removal, as is the case for CO and H_2. An obvious argument that may explain the relatively high observed efficiency for CO_2 is near-resonant frequency matching. CO_2 has relatively low-frequency bending (667 cm^{-1}) and symmetric stretching modes (1333 cm^{-1}). There is also a well-known Fermi interaction between them because $\omega_1 \approx 2\omega_2$.[56]

This results in a number of overtone and combination levels spanning energies above the ground state that are within a small multiple of kT of the CH A state $v = 1 \leftarrow 0$ energy gap (2740 cm^{-1}), a condition well-known to promote efficient resonant energy exchange.

Finally, we return to our primary interest in this work, the state-specific electronic coupling of the CH A and B states. Our results demonstrate clearly that this is a ubiquitous process, being measurable for all the quenchers we have examined. As we have noted previously for the specific case of CO_2, if it were neglected this could cause potentially serious errors of interpretation of data affected by quenching, for example, in the LIF probing of concentrations of CH in high-pressure environments. The current results extend this cautionary note to essentially all collision partners. This is particularly true of those such as the noble gases. Although these are correctly regarded as very inefficient quenchers of CH $A^2\Delta$, $v = 0$, at sufficiently high pressure they will cause appreciable conversion of $A^2\Delta$, $v = 1$ to $B^2\Sigma^-$, $v = 0$ and the reverse.

In a similar vein, our results for the B0 $\rightarrow$ A1/A0 branching caution further against the use of empirical energy gap scaling laws to estimate such vibrational branching ratios for electronic state-changing processes.[57,58] As has been pointed out before, there is no theoretical justification for their use in this context.[49,59,60] The very fact that the ratio is *collision-partner-dependent* immediately invalidates the use of relationships that focus only on the internal energy level structure or the Franck−Condon overlap in the molecule being relaxed. The value of the ratio predicted from a typical version of these relationships[49] favors the nearly degenerate A1 level by several orders of magnitude more than is observed for any of the partners. Although A1 is the dominant level in all cases, we can speculate that there may be some explanation for the partners that cause enhanced production of A0. The data for He are least certain because of the overall low transfer probability, but they seem to resemble the clearer results for Ar and N_2 that deposit only something around 10% of the population in A0. In contrast, for H_2, CO, and CO_2, this fraction is significantly higher at around 30−40%. For CO_2 at least, for which the measurements are not obscured by competition with much more rapid total removal, it is plausible that enhanced B0 $\rightarrow$ A0 production accompanies relatively efficient A1 $\rightarrow$ A0 vibrational relaxation. This would be consistent with a mechanism in which a nascent A1 molecule formed in a collision between B0 and CO_2 underwent secondary vibrational relaxation prior to escaping the collision complex. The other collision partners for which B0 $\rightarrow$ A0 production is relatively favorable, CO and H_2, also correspond to those with rapid total removal rate constants. We do not speculate on whether this is a coincidence other than to note that this is still a long way away from the statistical limit associated with strong complex formation. We reiterate that it is difficult to test the argument just suggested for CO_2 because of the practical difficulty in measuring A1 $\rightarrow$ A0 vibrational relaxation rate constants for these partners, as discussed above.

Returning to the absolute values of the B $\leftrightarrow$ A transfer rate constants, we draw a significant conclusion that there is a trend in Table 1 toward more efficient transfer for the more polarizable partners. We have attempted to put this on a more quantitative footing through the construction of a correlation plot of the well-established Parmenter−Seaver type.[61] In brief, this procedure relates the cross section (in the present case, thermally averaged values, $\langle\sigma\rangle$) to the attractive well depth for pairs of quencher molecules, ϵ_{QQ}. It is justified on the basis that the unknown well depth, ϵ_{AQ}, between the molecule being quenched (in this case CH (A or B)) and the collision partner can be reasonably approximated by the geometric average of ϵ_{QQ} and that (also unknown) for pairs of collision partners, ϵ_{AA}. The anticipated exponential dependence of the cross section on ϵ_{AQ} leads to a logarithmic proportionality on $\sqrt{\epsilon_{QQ}}$, conventionally expressed as

$$\ln(\langle\sigma\rangle) \propto \left(\frac{\epsilon_{QQ}}{k}\right)^{1/2} \tag{9}$$

where k is the Boltzmann constant.

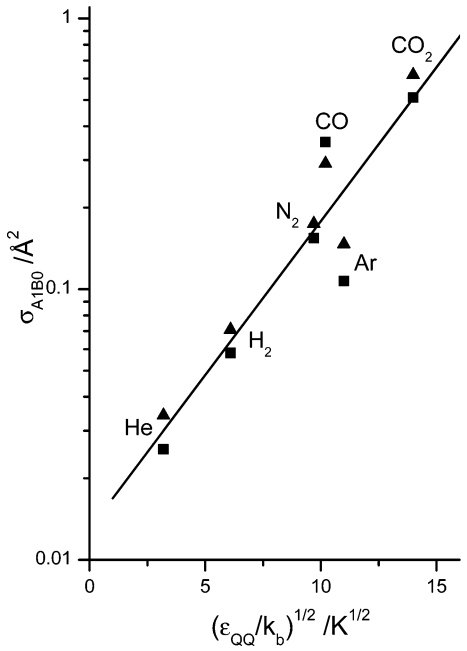

Figure 11. Parmenter−Seaver plot showing the correlation of the thermally averaged cross section for CH A1 $\rightarrow$ B0 transfer with long-range attractive forces as measured by the well depth of pairs of collision partners. Triangles represent σ_{A1B0} data obtained from experiments where the A1 level was initially pumped. Squares represent σ_{A1B0} data obtained from experiments where B0 was pumped.

The corresponding correlation plot for A1 $\rightarrow$ B0 transfer is shown in Figure 10. (Since microscopic reversibility is reasonably consistently obeyed, a qualitatively similar but somewhat more scattered plot is also obtained for the corresponding reverse process.) The independently derived results for both A1 and B0 pumping are shown in Figure 11 for comparison. We conclude that there is indeed a very plausible positive correlation between the efficiency of CH A $\leftrightarrow$ B state coupling and long-range attractive forces.

There have been a number of previous attempts,[16] with very limited success, to identify similar and related correlations for *total* removal rate constants for the CH (A) state (and other diatomic hydrides). There has also been considerable related discussion of multipole models of attractive forces which attempt to explain the rotational level dependence of total quenching.[16,29,33,39,41,47,48,62] We believe this is the first time that the Parmenter−Seaver approach has been applied to a *specific electronic channel* for CH. An immediate practical implication of the apparent positive correlation is that it should provide a simple method for predicting the relative efficiencies of CH B $\leftrightarrow$ A coupling for other (unmeasured) partners, at least at a fixed temperature. At a more fundamental level, it provides some insight into the mechanism for this collision-induced change of electronic state. As we have noted previously,[49] ab initio studies[5] of CH indicate the dominant electronic configurations for these two states in the region of the equilibrium internuclear

separation. The $A^2\Delta$ state is best described as $1\sigma^2 2\sigma^2 3\sigma^1$ ($1\pi^2$, $^1\Delta$). The $B^2\Sigma^-$ state is correspondingly $1\sigma^2 2\sigma^2 3\sigma^1$ ($1\pi^2$, $^3\Sigma^-$). A ↔ B conversion therefore involves a reorganization of the electrons in the π orbitals, maintaining an overall doublet spin state. As has been discussed extensively in the context of other related diatomic molecules,[62] states which do not interact to high order in the isolated molecule (in this case because $\Delta\Lambda = 2$) may be mixed by the electrostatic interaction with the collision partner in the reduced symmetry of the collision pair.

It might perhaps be surprising at first sight that this mixing does *not* appear to be enhanced by the strong chemical interactions present for some of the collision partners. In particular, as noted above, there are deeply bound CH_3 and HCCO intermediates on the respective CH + H_2 and CH + CO surfaces. The presence of such complexes has, for example, been demonstrated previously to provide a highly efficient mechanism for *vibrational* relaxation in the electronic ground state of related simple radicals, such as OH.[63] Indeed, this has become the basis of a widely discussed method for estimating the total capture rate constant for complex formation in such recombination reactions. However, inspection of Figure 9 shows that CH B ↔ A electronic coupling efficiencies of H_2 and CO do not lie significantly out of line with the trend established by the other partners, including those for which chemical reaction and deeply bound intermediates are clearly not a possibility. A reasonable interpretation of the successful Parmenter−Seaver correlation is that the efficiency of B ↔ A interconversion is related to the long-range capture probability that is mediated by relatively weak dispersive attractive interactions. The implication of our results is that the much stronger, shorter-range, chemically specific interactions do not further enhance this specific process.

In fact, though, there is some previous independent experimental evidence consistent with this argument. It has been observed that at least some channels on the CH_3 and HCCO surfaces are *not* characterized by strong CH A ↔ B mixing. In the vacuum ultraviolet (VUV) photodissocation of the CH_3 radical,[64] resonances associated with CH_3 Rydberg states produce CH $A^2\Delta$ as the dominant electronically excited product. Even above the threshold for $B^2\Sigma^-$ production, it is formed in much lower yield. This suggests that A ↔ B mixing in the exit channel of these surfaces is weak. The reverse capture process of the $A^2\Delta$ state in collision with H_2 may proceed initially over the same Rydberg surfaces but then consistently lead to products other than the $B^2\Sigma^-$ state, most likely CH_2 + H, due to crossings at shorter range. Collisions of CH $B^2\Sigma^-$ with H_2 presumably proceed over a different family of entrance channel surfaces that are only weakly coupled to the $A^2\Delta$ state and not accessed via photoexcitation from ground-state CH_3. Similarly, the important combustion reaction $O(^3P)$ + C_2H via the HCCO surface produces CO + CH predominantly in the $A^2\Delta$ state.[65] Once again, there is apparently no strong coupling to surfaces leading asymptotically to the CH $B^2\Sigma^-$ state, at least in the regions explored by this reaction.

We hope that the new insight provided by our results into the mechanism of the collisional coupling of the CH A and B states will stimulate further theoretical work characterizing the topology of the electronic surfaces for these systems and the couplings between them.

Acknowledgment. We acknowledge the contributions of Florian Ausfelder, Colin Randall, and Craig Murray to earlier phases of this work. We thank the EPSRC for an equipment grant and for studentship funding for G.R. M.L.C thanks the Royal Society of Edinburgh for a BP Research Fellowship.

References and Notes

(1) Bernath, P. F. *J. Chem. Phys*. **1987**, *86*, 4838−4842.
(2) Bernath, P. F.; Brazier, C. R.; Olsen, T.; Hailey, R.; Fernando, W. T. M. L.; Woods, C.; Hardwick, J. L. *J. Mol. Spectrosc*. **1991**, *147*, 16−26.
(3) Zachwieja, M. *J. Mol. Spectrosc*. **1995**, *170*, 285−309.
(4) Kepa, R.; Para, A.; Rytel, M.; Zachwieja, M. *J. Mol. Spectrosc*. **1996**, *178*, 189−193.
(5) van Dishoeck, E. F. *J. Chem. Phys*. **1987**, *86*, 196.
(6) Kalemos, A.; Mavridis, A.; Metropoulos, A. *J. Chem. Phys*. **1999**, *111*, 9536−9548.
(7) Rensberger, K. J.; Jeffries, J. B.; Copeland, R. A.; Köhse-Hoinghaus, K.; Wise, M. L.; Crosley, D. R. *Appl. Opt*. **1989**, *28*, 3556−3566.
(8) Luque, J.; Crosley, D. R. *Appl. Opt*. **1999**, *38*, 1423−1433.
(9) Allen, M. G.; Howe, R. D.; Hanson, R. K. *Opt. Lett*. **1986**, *11*, 126−128.
(10) Donbar, J. M.; Driscoll, J. F.; Carter, C. D. *Combust. Flame* **2000**, *122*, 1−19.
(11) Chen, Y.-C.; Mansour, M. S. *Appl. Phys. B* **1997**, *64*, 599−605.
(12) Luque, J.; Crosley, D. R. *Appl. Phys. B* **1996**, *63*, 91−98.
(13) Luque, J.; Klein-Douwel, R. J. H.; Jeffries, J. B.; Smith, G. P.; Crosley, D. R. *Appl. Phys. B* **2002**, *75*, 779−790.
(14) Luque, J.; Berg, P. A.; Jeffries, J. B.; Smith, G. P.; Crosley, D. R.; Scherer, J. J. *Appl. Phys. B* **2004**, *78*, 93−102.
(15) Luque, J.; Berg, P. A.; Jeffries, J. B.; Smith, G. P.; Crosley, D. R.; Sherer, J. J. *Appl. Phys. B* **2004**, *78*, 93−102.
(16) Tamura, M.; Berg, P. A.; Harrington, J. E.; Luque, J.; Jeffries, J. B.; Smith, G. P.; Crosley, D. R. *Combust. Flame* **1998**, *114*, 502−514.
(17) Joklik, R. G.; Daily, J. W. *Combust. Flame* **1987**, *69*, 211−219.
(18) Becker, K. H.; Brenig, H. H.; Tatarczyk, T. *Chem. Phys. Lett*. **1980**, *71*, 242−245.
(19) Nokes, C. J.; Gilbert, G.; Donovan, R. J. *Chem. Phys. Lett*. **1983**, *99*, 491−493.
(20) Nokes, C. J.; Donovan, R. J. *Chem. Phys*. **1984**, *90*, 167−174.
(21) Garland, N.; Crosley, D. R. *Chem. Phys. Lett*. **1987**, *134*, 189−194.
(22) Heinrich, P.; Kenner, R. D.; Stuhl, F. *Chem. Phys. Lett*. **1988**, *147*, 575−580.
(23) Bauer, W.; Engelhardt, B.; Wiesen, P.; Becker, K. H. *Chem. Phys. Lett*. **1989**, *158*, 321−324.
(24) Kenner, R. D.; Pfannenberg, S.; Heinrich, P.; Stuhl, F. *J. Phys. Chem*. **1991**, *95*, 6585−6593.
(25) Chen, C.; Wang, X.; Yu, S.; Lu, Q.; Ma, X. *Chem. Phys. Lett*. **1992**, *197*, 286−291.
(26) Chen, C.; Ran, Q.; Yu, S.; Ma, X. *J. Chem. Phys*. **1993**, *99*, 1070−1075.
(27) Heinrich, P.; Stuhl, F. *Chem. Phys*. **1995**, *199*, 105−118.
(28) Heinrich, P.; Stuhl, F. *Chem. Phys*. **1995**, *199*, 297−304.
(29) Chen, C.; Wang, F.; Chen, Y.; Ma, X. *Chem. Phys*. **1998**, *230*, 317−325.
(30) Cerezo, C.; Martin, M. *J. Photochem. Photobiol., A* **2000**, *134*, 127−132.
(31) Chen, C.; Ran, Q.; Yu, S.; Ma, X. *Chem. Phys. Lett*, **1993**, *203*, 307−313.
(32) Chen, C.; Sheng, Y.; Yu, S.; Ma, X. *J. Chem. Phys*. **1994**, *101*, 5727−5730.
(33) Cooper, J. L.; Whitehead, J. C. *J. Chem. Soc., Faraday Trans*. **1992**, *88*, 2323−2327.
(34) Garland, N.; Crosley, D. R. *Appl. Opt*. **1985**, *24*, 4229−4237.
(35) Rensberger, K. J.; Dyer, M. J.; Copeland, R. A. *Appl. Opt*. **1988**, *27*, 3679−3689.
(36) Luque, J.; Crosley, D. R. *Appl. Opt*. **1999**, *38*, 1423−1433.
(37) Luque, J.; Klein-Douwel, R. J. H.; Jeffries, J. B.; Crosley, D. R. *Appl. Phys. B* **2000**, *71*, 85−94.
(38) Bütler, A.; Rahmann, U.; Köhse-Hoinghaus, K.; Brockhinke, A. *Appl. Phys. B* **2004**, *79*, 113−120.
(39) Dixon, R. N.; Newton, D. P.; Rieley, H. *J. Chem. Soc., Faraday Trans. 2* **1987**, *83*, 675−682.
(40) Cooper, J. L.; Whitehead, J. C. *J. Chem. Soc., Faraday Trans*. **1993**, *89*, 1287−1290.
(41) Cooper, J. L.; Whitehead, J. C. *J. Phys. Chem*. **1994**, *98*, 8274−8278.
(42) Wang, C.-C.; Chen, Y. P.; Chin, T. L.; Huang, H. Y.; Lin, K. C. *J. Chem. Phys*. **2000**, *112*, 10204−10211.
(43) Kind, M.; Stuhl, F. *J. Chem. Phys*. **2001**, *114*, 6160−6165.
(44) Kind, M.; Stuhl, F.; Tzeng, Y.-R.; Alexander, M. H.; Dagdigian, P. J. *J. Chem. Phys*. **2001**, *114*, 4479−4489.
(45) Nizamov, B.; Dagdigian, P. J.; Tzeng, Y.-R.; Alexander, M. H. *J. Chem. Phys*. **2001**, *115*, 800−809.

(46) Crichton, H. J.; Murray, C.; McKendrick, K. G. *Phys. Chem. Chem. Phys*. **2002**, *4*, 5768−5777.
(47) Meden, P.; Kind, M.; Stuhl, F. *J. Chem. Phys.* **2002**, *116*, 2757−2762.
(48) Kind, M.; Meden, P.; Stuhl, F. *J. Chem. Phys.* **2002**, *117*, 11152−11157.
(49) Randall, C. J.; Murray, C.; McKendrick, K. G. *Phys. Chem. Chem. Phys.* **2000**, *2*, 461−471.
(50) Murray, C.; Randall, C. J.; McKendrick, K. G. *Phys. Chem. Chem. Phys*. **2000**, *2*, 5553−5559.
(51) Taatjes, C. A. *J. Chem. Phys*. **1997**, *106*, 1786−1795.
(52) Luque, J.; Crosley, D. R. *LIFBASE: Database and Spectral Simulation Program*, version 1.5; SRI International Report MP 99-009; SRI International: Menlo Park, CA, 1999.
(53) *Microcal Origin 6.0, Implementing a Levenberg−Marquardt Nonlinear Least Squares Method*; Microcal Software Inc.: Northaptom, MA, 1999.
(54) Luque, J.; Crosley, D. R. *J. Chem. Phys*. **1996**, *104*, 2146−2155.
(55) Luque, J.; Crosley, D. R. *J. Chem. Phys*. **1996**, *104*, 3907−3913.
(56) Tashkun, S. A.; Perevalov, V. I.; Teffo, J.-L.; Rothman, L. S.; Tyuterev, Vl. G. *J. Quant. Spectosc. Radiat. Transfer* **1998**, *60*, 785−801.
(57) Katayama, D. H.; Miller, T. A.; Bondybey, V. E. *J. Chem. Phys*. **1979**, *71*, 1662−1669.
(58) Bondybey, V. E.; Miller, T. A. *J. Chem. Phys*. **1978**, *69*, 3597−3602.
(59) Dagdigian, P. J. *Annu. Rev. Phys. Chem*. **1997**, *48*, 95−123.
(60) McKendrick, K. G. *J. Chem. Soc., Faraday Trans.* **1998**, *94*, 1921−1932.
(61) Lin, H.-M.; Seaver, M.; Tang, K. Y.; Knight, A. E. W.; Parmenter, C. S. *J. Chem. Phys*. **1979**, *70*, 5442−5457.
(62) Crosley, D. R. *J. Phys. Chem*. **1989**, *93*, 6273−6282.
(63) Smith, I. W. M. S. *J. Chem. Soc., Faraday Trans*. **1997**, *93*, 3741−3750.
(64) Kassner, Ch.; Stuhl, F. *Chem. Phys. Lett*. **1994**, *222*, 425−430.
(65) Devriendt, K.; Van Look, H.; Ceursters, B.; Peeters, J. *Chem. Phys. Lett*. **1996**, *261*, 450−456.